Grant agreement no: 257856

SiNAPS

Semiconducting Nanowire Platform for Autonomous Sensors

Collaborative Project
FP7-ICT-2009-5: Future and Emerging Technologies
"Towards Zero Power ICT" Proactive Scheme

D1.2: p-n junction properties of single core-shell NWs

Due date of deliverable: M18 Actual submission date: 09/02/2012

Start date of project: 01 Aug 2010 Duration: 36 months

Lead contractor for this deliverable: Tyndall Revision: V.1.0

Project co-funded by the European Commission within the 7th Framework Programme (2007-2013)		
Dissemination Level		
PU	Public	
PP	Restricted to other programme participants (including the Commission Services)	
RE	Restricted to a group specified by the consortium (including the Commission Services)	
CO	Confidential, only for members of the consortium (including the Commission Services)	CO

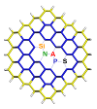

1 Executive Summary

Silicon nanowire (SiNW) solar cells were prepared using silicon nanowire arrays etched into a slightly doped silicon wafer and CVD-grown silicon nanowires. The sample preparation is detailed in the SiNAPS deliverable reports D1.1 and D1.3.

A hetero-junction to amorphous silicon was generated by depositing hydrogenated amorphous silicon by PECVD as a shell around the nanowires. The p-n junction structure was investigated by high resolution lattice imaging on a TEM. A comparison between structural properties of the p-n junction NWs prepared by CVD growth and metal-assisted etching is demonstrated, highlighting the importance of the structural characterisation for guiding the development of high-efficiency solar cells. Locally p-n junctions were visualised by EBIC (electron beam induced current) measurements on p-n junction NW arrays. A method for single NW p-n junction characterisation using nano-manipulator in conjunction with single NW EBIC measurements is being developed. Such measurements will correlate structural properties of the p-n junction NWs with their electrical performance.

2 Preparation of Samples

The preparation of SiNW solar cells by metal-assisted etching on n-doped silicon wafers is described in detail in the SiNAPS Deliverable D1.1 ‘1st batch of NW-modified energy harvesting’.

The preparation of SiNW arrays by self-organized vapor liquid solid (VLS) growth in a cold wall UHV chemical vapor deposition (CVD) reactor is described in detail in the SiNAPS Deliverable D1.3 ‘Structural and electrical properties of integrated core-shell nanowire arrays’.

3 Structural Properties of p-n junctions

Since the junction formation, in contrast to the traditional implantation route, in our work is a result of growth (or etching) processes (e.g. for the formation of the n-type core) followed by p-type a-Si deposition, it is imperative to obtain detailed understanding of the p-n junction interface. Possible variations both in the uniformity of the junction and dopant incorporation can have erratic implications upon p-n junction performance (carrier separation and recombination processes) and corresponding PV output.

Initial structural characterisation of the NW arrays was done by top down and tilts view SEM. Detailed structural analysis of the p-n junction interface on isolated structures was performed using cross-sectional TEM analysis in longitudinal (along NWs long axis) and transverse directions. Thus information regarding the uniformity of the interface, thickness variations and homogeneity of the p-n junction interface was obtained. Further visualisation of the p-n junction interface was obtained by lattice imaging using high resolution TEM. This type of analysis was possible by developing an original TEM sample preparation routine based on in-situ lift out process within a Dual Beam FIB/SEM system. The key to success of the developed procedure is in deposition of protective layers and final thinning at oblique angles using low kV Ga-ion beams. We have analysed and contrast samples from (i) CVD grown SiNW arrays and (ii) etched SiNWs via metal assisted process.

3.1 CVD-grown SiNW arrays

Figure 1 describes the surface of n-type CVD grown SiNWs after p-type a-Si deposition (a and b) and after subsequent AZO deposition (c and d). It is clear that the surface of the NWs is significantly rougher than what is expected for atomically flat interface. This erratic behaviour can be a result of (i) the growth process of the n-doped core SiNW and/or (ii) subsequent p-type a-Si deposition process. Most importantly the AZO was deposited conformally forming poly-crystalline contact. In order to address the issue of the high surface roughness of the grown SiNWs, and the possible influence on p-n junction interface TEM analysis was undertaken.

Figure 2 a shows a cross-sectional TEM image of a typical n-type Si NW core and p-type a-Si imaged in a transverse direction. Using such imaging condition direct identification of the n-type Si core and p-type a-Si can be obtained. It is seen that there is a thickness variation in the deposition of the a-Si, (thicker deposition on the top side of the SiNW). This can be explained by the directionality of the deposition process, as opposed to conformal coating. When imaged in the longitudinal direction any variation in uniformity of p-n junction interface along the NW long axis can be obtained (see Figure 2 b). It is seen that the NW surface is forming so called saw-tooth interface which is a result of the growth process. Thus the question regarding the roughness of the SiNWs can be answered e.g. the uniformity of the p-n junction interface is ruled out by the fact that crystalographically uneven surface is formed during the NWs growth process.

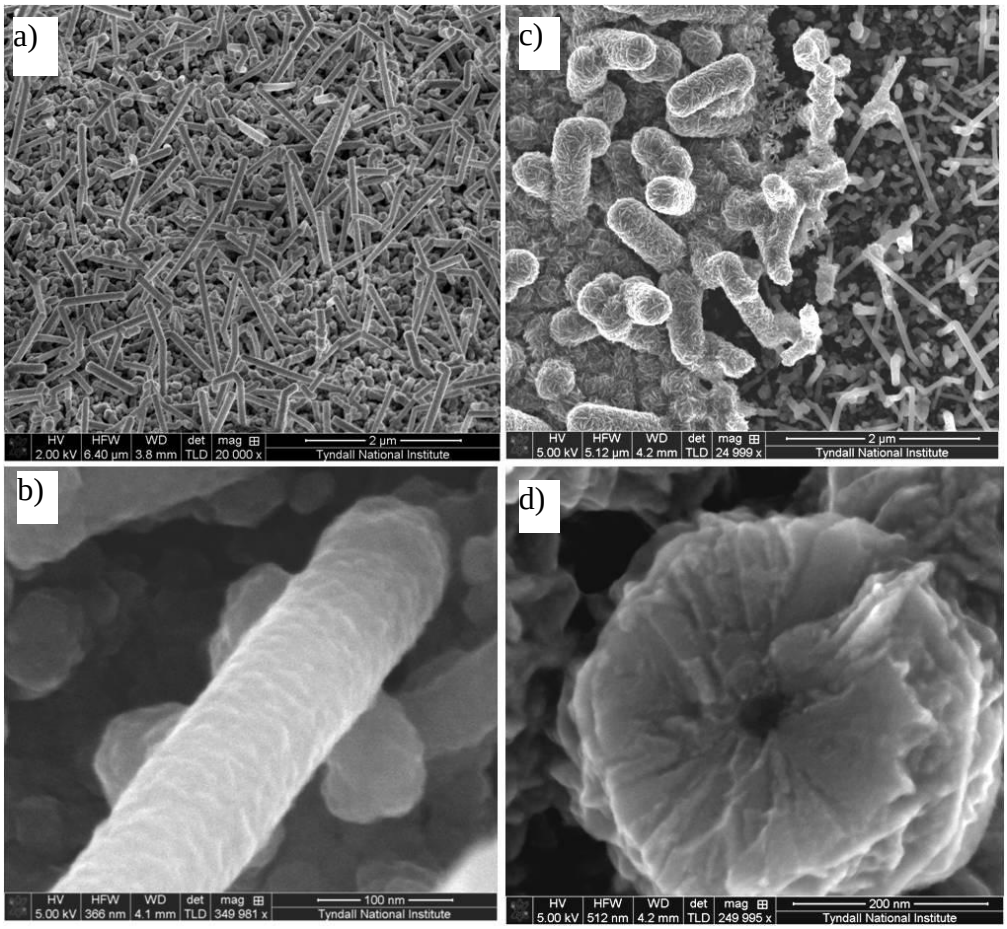

Figure 1. Top-down SEM images of CVD grown n-type SiNWs with p-type a-Si shells (a and b), and same after ALD deposition of the transparent AZO contact (c and d).

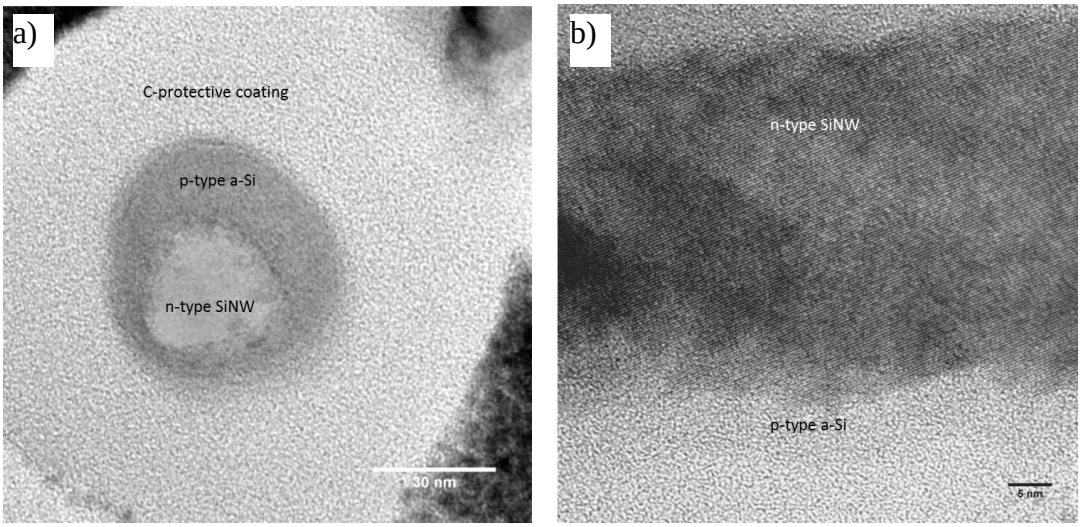

Figure 2. TEM images of CVD grown n-type SiNWs with p-type a-Si shells, in a transverse a) and longitudinal b) directions.

3.2 Metal-assisted etched SiNW arrays

Metal assisted etching offers the possibility of fast and inexpensive formation of Si NWs. Moreover the doping (possible clustering and non-uniform dopant profiles) of the NWs does not depend on the growth conditions as it is the case of grown SiNWs. Unfortunately, strict control over the NWs shapes and diameters cannot be attained. The aim of the structural study herein was to determine the uniformity of the p-n junction interface, that can be influenced by (i) the etching conditions used to form the n-type core Si NWs and (ii) p-type a-Si deposition (two different dopant concentrations were introduced during the a-Si deposition).

Figure 3 shows top down SEM images of etched Si NWs that were subjected to a-Si deposition at low and high B-content. It is clear that there is a substantial increase in the surface roughness of p-type shell deposited at high B-content. This can result in increased carrier trapping and recombination during the PV performance and pin-points the fact that detail understanding of the structural properties is essential.

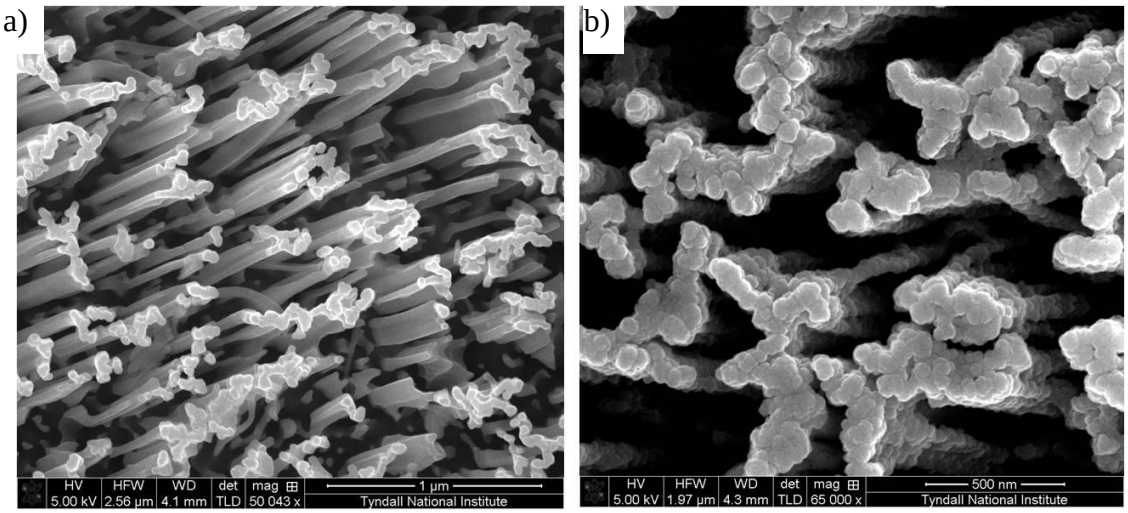

Figure 3. Top down SEM images of n-type Si NW arrays produced by metal-assisted chemical etching and subjected to p-type a-Si deposition at low a) and b) high B-content during the PECVD process.

Figure 4 depicts the two cross-sectional TEM images (in longitudinal and transverse direction) of etched n-type SiNWs coated with a-Si shells deposited at low B-concentration. It is seen that the SiNW surface is relatively smooth (improved surface roughness in comparison to CVD grown SiNWs) forming uniform p-n junction interface. In comparison to the grown SiNWs, metal-assisted process results in “star”-like or sometimes fully irregular NW cross-section (as seen by the transverse direction TEM image, Figure 4 b). Notably, to the best of our knowledge, this is the first time that SiNWs prepared by metal assisted etching are imaged in such an orientation by TEM. Unfortunately, the formation of the p-type a-Si shell, suffers from considerable thickness variations (similar observation was seen for the CVD SiNWs) both along

the NW length and in their radial direction. As outlined previously this is a result of the directional (as oppose to conformal) a-Si deposition by PECVD. Substantial difference in comparison to CVD grown NWs, is that the metal-assisted etched SiNWs are bundling at the top forming aggregates that are bringing additional shadowing during the deposition. Thus a-Si "caps" are formed on top of the NWs with much higher thickness then the a-Si on the NWs side facets (see Figure 4 c and d). Most importantly the p-type a-Si/ n-type core SiNW is almost atomically flat as seen by the lattice imaging HRTEM (see Figure 5). Such type of interface is beneficial for reduced surface trapping and recombination of the minority carriers, and can have much importance in understanding the overall PV behaviour of the structures.

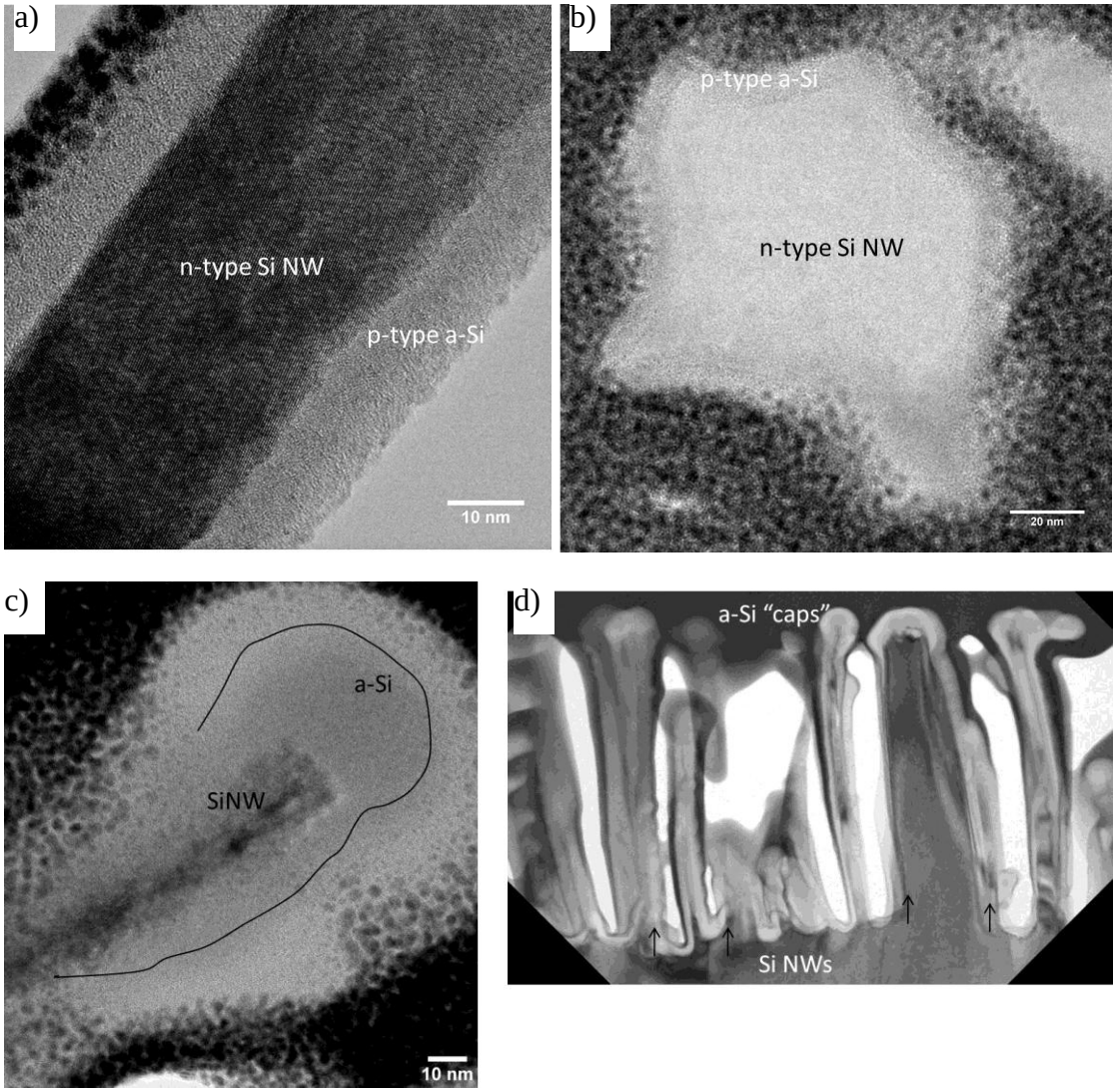

Figure 4. TEM images of typical etched SiNWs with p-type a-Si shells imaged in longitudinal a) and transverse b) directions, and cross-sectional TEM images depicting variation in the thickness of the a-Si shell and formation of a-Si "caps" c) and d).

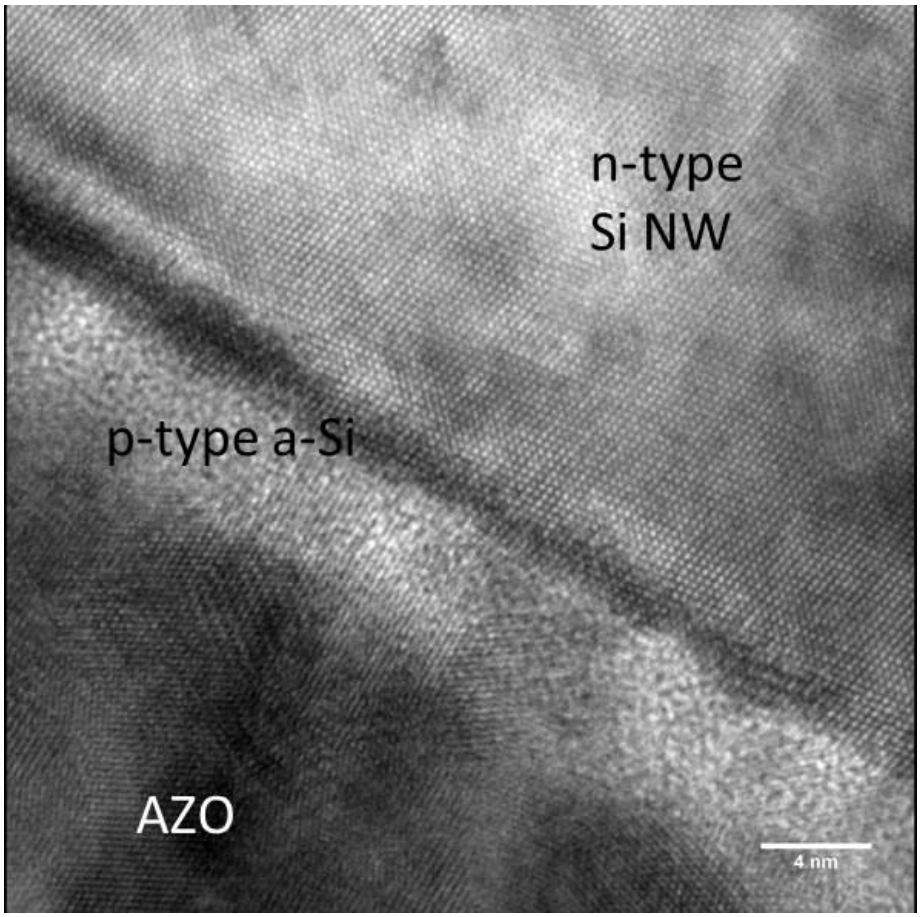

Figure 5. HRTEM image of p-n junction interface demonstrating almost atomically flat interface.

4 Local p-n junction properties by EBIC

In EBIC (electron beam induced current) the current in a solar cell is generated by a focussed electron beam of a SEM. The principle of EBIC is based on the electric field present in the depletion region of a Schottky or p-n junction. The electron beam of the SEM is scanning over the sample, inducing electron-hole pairs in the semiconductor. In the absence of an electric field, these eventually recombine. But if the induced charge carriers diffuse into the depletion region of a junction, the electric field separates them yielding a net current when the circuit is closed. The magnitude of the induced current at each pixel is represented by different gray levels in the EBIC image. For orientation, the EBIC image is always shown next to a secondary electron (SE) image of the same location and with the same magnification. Due to the limited penetration depth of the primary electron beam, the carriers are generated in a surface near layer of the material. Only recently, EBIC has been used to visualise and understand diffusion of carries of axial p-n junction SiNWs. Herein by choosing appropriate conditions, we can verify and visualize the functionality of the solar cells by EBIC measurements.

4.1 EBIC of arrays of p-n junction Si-NWs

At an accelerating voltage of 10 kV, the penetration depth of the primary electrons, incidenced on top of the p-n junction SiNWs (see Figure 6), is less than 800 nm in case of the solar cells with 200 nm AZO. Therefore, the carriers are generated within the nanowires, and can quickly be separated by the electrical field of the space charge region of the core-shell solar cells. Consequently the EBIC current measured originate mainly from the nanowires. Fig. 6 demonstrates the EBIC and the corresponding secondary electron (SE) images at the same region (upper images) and the magnified images (lower images) in the regions marked with red rectangles. The images indicate that the EBIC signal at the NWs (green circles) is lower than the one measured at holes (blue circle). In a standard diode measurement set-up, the EBIC signal can be understood by considering that in p-type shell/n-type core junction configuration the carriers' separation is such that electrons are collected in the direction of the Si wafer substrate and the holes are collected at the top AZO electrode. In this case positive EBIC current is expected that is shown by darker pixels.

The EBIC is at least one order higher than the beam current, which unambiguously demonstrates that the nanowires work as active PV component. It is noted that for conventional solar cells, the EBIC signal is usually 3 orders higher than the beam current at 10 kV. The lower EBIC in the case of the NWs solar cell is a result of the surface geometric structure, the thick AZO layer, reduced carrier generation in the NWs and probable surface recombination.

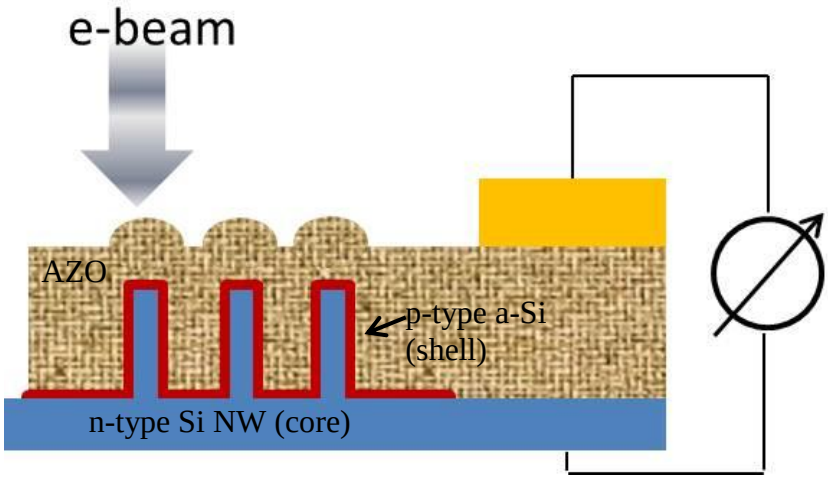

Figure 6. Schematics of the experimental set-up for top down EBIC measurments of core-shell p-n junction Si NW devices.

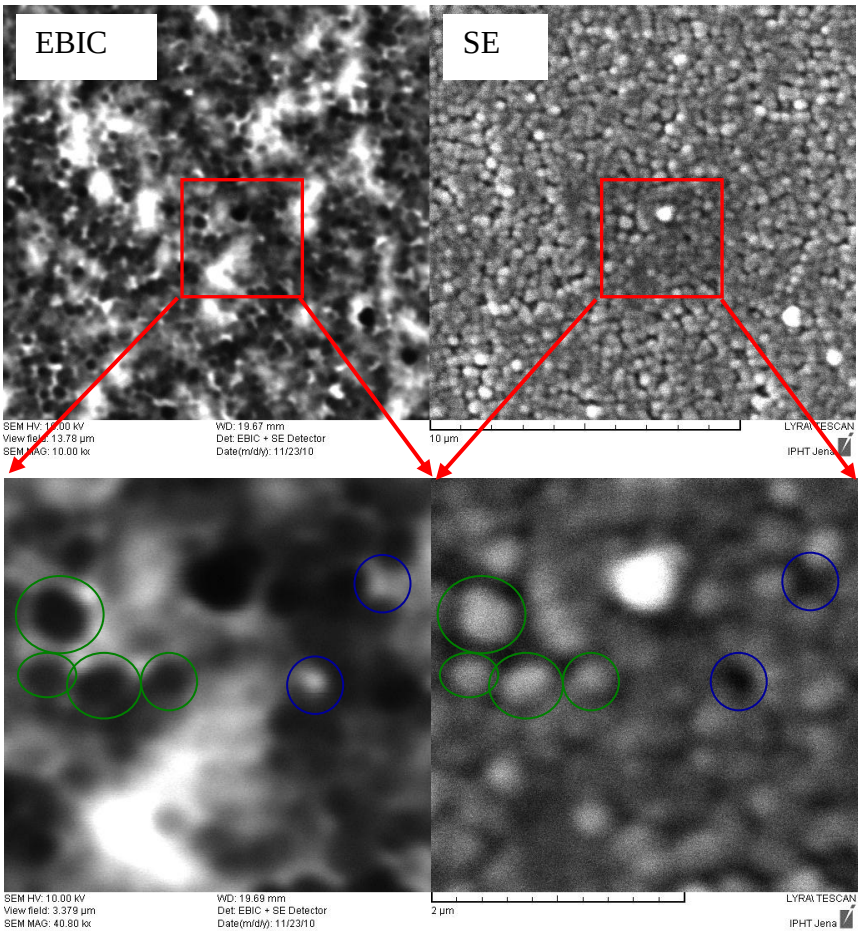

Figure 7. EBIC and SE images (upper) taken at a beam energy of 10 kV, and the corresponding magnified images (lower) in the region marked as red rectangles. The green circles marked the NWs and the blue ones the holes.

4.2 EBIC of single p-n junction Si-NWs

The proposed architecture of the set is shown in Figure 6. The method is based on the single NW contacting using nano-manipulators and simultaneous EBIC measurements. It is anticipated that by using the electron beam probe in side-view geometry and localising the measurements on a single NW will allow for visualisation of the p-n junction interface in the EBIC map. Furthermore using site specific TEM sample preparation on a Dual Beam FIB system, TEM thin foil incorporating the same device can be extracted. In this way both high resolution structural and EBIC performance can be correlated.

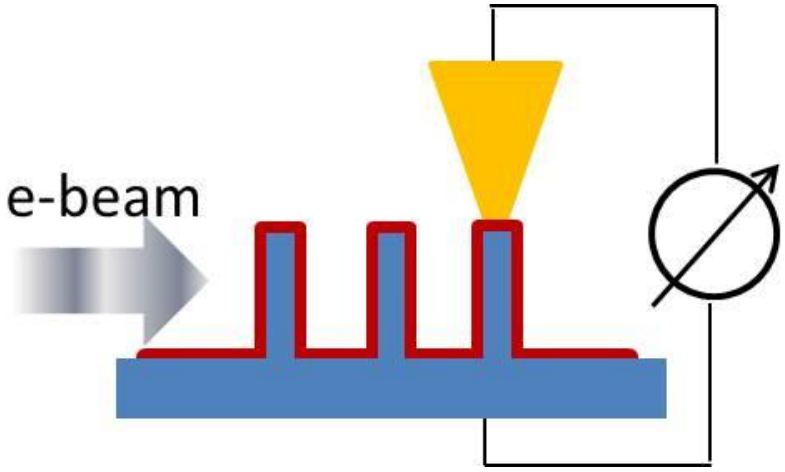

Figure 6. Schematics of the experimental set-up for side view, single NW EBIC measurements of core-shell p-n junction Si NW devices.

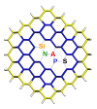

4 Summary, conclusions and outlook

Efficient core-shell AZO/a-Si/SiNWs p-n junction solar cells have been successfully fabricated and the properties of the p-n junction interface investigated by HRTEM and EBIC experiments. Based on such characterisation a comparison between structural properties of the p-n junction NWs prepared by CVD growth and metal-assisted etching is demonstrated, highlighting the importance of structural features in the expected solar cell performance.

EBIC measurements of p-n junction arrays demonstrate that the active part of the NW solar cells is indeed the NW p-n junction structures. Detailed understanding of the electrical properties of single p-n junction NW devices will be investigated by the newly developed EBIC technique using nano-manipulators. This will give further insight into the mechanism of carriers separation, possible surface recombination and trapping.

References

[1] E.C. Garnett and P. Yang. Silicon Nanowire Radial p- n Junction Solar Cells. *Journal of the American Chemical Society*, **130** (29): 9224–9225, 2008.

[2] Q. Wang, MR Page, E. Iwaniczko, Y. Xu, L. Roybal, R. Bauer, B. To, H.C. Yuan, A. Duda, F. Hasoon, et al. Efficient heterojunction solar cells on p-type crystal silicon wafers. *Applied Physics Letters*, **96**: 013507, 2010.

[3] V. Sivakov, G. Andrä, A. Gawlik, A. Berger, J. Plentz, F. Falk, and SH Christiansen. Silicon Nanowire-Based Solar Cells on Glass: Synthesis, Optical Properties, and Cell Parameters. *Nano Lett*, **9** (4): 1549–1554, 2009.

[4] R.S. Wagner and W.C. Ellis. Vapor-Liquid-Solid Mechanism of Single Crystal Growth. *Applied Physics Letters*, **4**: 89, 1964.

[5] T. Stelzner, G. Andrä, E. Wendler, W. Wesch, R. Scholz, U. Gösele, and S. Christiansen. Growth of silicon nanowires by chemical vapour deposition on gold implanted silicon substrates. *Nanotechnology*, **17**: 2895–2898, 2006.

[6] T.J. Kempa, B. Tian, D.R. Kim, J. Hu, X. Zheng, and C.M. Lieber. Single and Tandem Axial pin Nanowire Photovoltaic Devices. *Nano Letters*, **8** (10): 3456–3460, 2008.

[7] T I Kamins, X. Li, R.S. Williams, and X. Liu. Growth and structure of chemically vapor deposited Ge nanowires on Si substrates. *Nano Letters*, **4** (3): 503–506, 2004.

[8] A. Lugstein, M. Steinmair, YJ Hyun, G. Hauer, P. Pongratz, and E. Bertagnolli. Pressure-induced orientation control of the growth of epitaxial silicon nanowires. *Nano letters*, **8** (8): 2310–2314, 2008.

[9] J. E. Allen, E. R. Hemesath1†, D. E. Perea1, J. l. Lensch-Falk1, Z.Y. li, F. Yin, M. H. Gass3, P. Wang, A. l. Bleloch, R. E. Pallmer and L. J. Lauhon. High-resolution detection of Au catalyst atoms in Si nanowires. *Nature Nanotechnology*, 3 (3): 168, 2008.

[10] S. Hoffmann, J. Bauer, C. Ronning, Th. Stelzner,|J. Michler, C. Ballif, V. Sivakov and S. H. Christiansen. Axial p-n Junctions Realized in Silicon Nanowires by Ion Implantation, *Nano Lett.* 9 (4): 1341-1344, 2009.

[11] J. Bauer, F. Fleischer, O. Breitenstein, L. Schubert, P. Werner, U. Gösele and M. Zacharias. Electrical properties of nominally undoped silicon nanowires grown by molecular-beam epitaxy. *Appl. Phys. Lett.*, **90**, 012105, 2007.